Chapter 4

Development of dye-sensitized solar cells based on gold (Au)/gelatin gel electrolyte: effect of different aspect ratio of Au nanorods

GRAPHICAL ABSTRACT

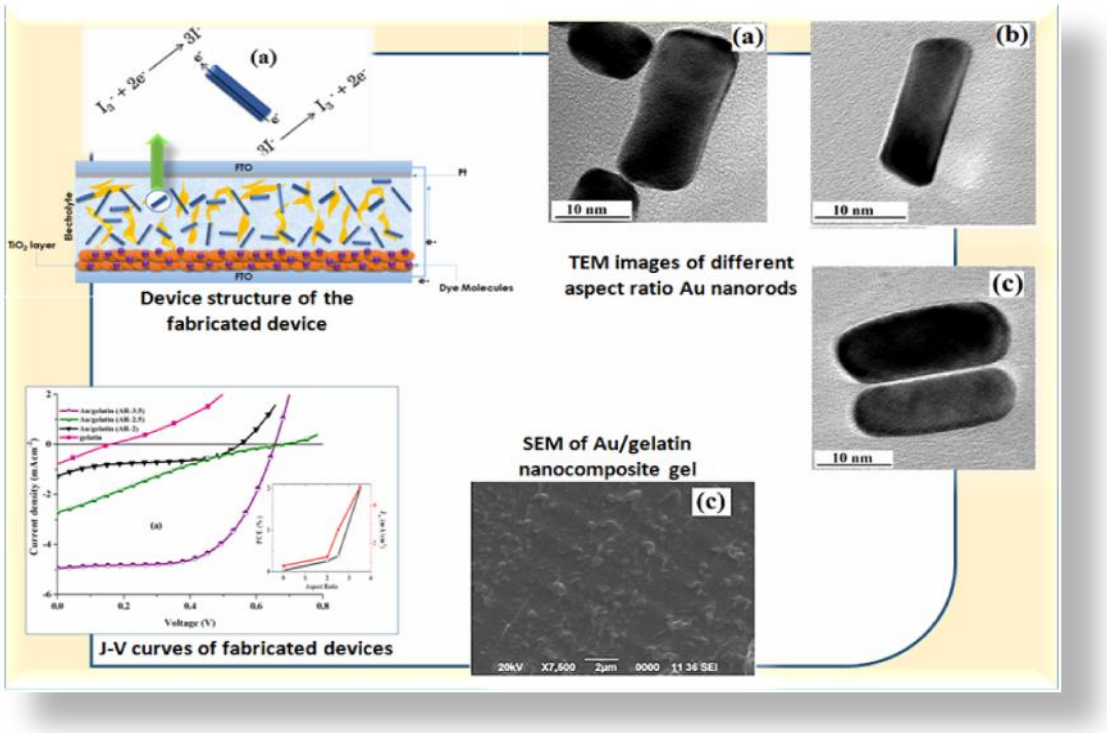

The high aspect ratio Au nanorods in the gel electrolyte offer high PCE in the DSSC thus providing remarkable electrocatalytic activity towards the redox reaction and reducing the charge transfer resistance in the electrolyte

4.1 Introduction

Dye-sensitized solar cells (DSSCs) offer a technically and economically plausible alternative way to fabricate modern photovoltaic devices. This type of device structure usually consists of a transparent electrode coated with a dye-sensitized mesoporous film of TiO_2 nanostructures, an electrolyte containing a suitable redox couple, and a metal (Pt) counter electrode. However, due to some problems related to encapsulation such as solvent leakage and evaporation caused by the use of the liquid electrolyte in conventional DSSCs, much work is being done to eliminate such demerits.[1-3] One of the modified and promising substitutes is the polymer gel electrolyte where the liquid electrolyte is entrapped in three dimensional network of a host polymeric gel. This can overcome the problem of electrolyte leakage and evaporation.[4]. Moreover, ions of the electrolyte can easily move in the solution phase, which provides a remarkable increase in ionic conductivity. DSSCs made up of polymer gel electrolytes are superior to conventional liquid electrolyte devices in the context of a solvent-free device that can provide improved thermal and long-term durability, higher environmental safety under breakage of the device, and so forth. Numerous examples are found on various polymers and copolymers that can be used to prepare a polymer gel electrolyte suitable for DSSCs.[5, 6] However, the polymer gel electrolytes have some drawbacks regarding their ionic conductivity which make them lower to their liquid counterparts, causing low device performance. Additionally, they have the low penetration into the mesoporous TiO_2 electrode due to which dyes cannot be sufficiently utilized due to the poor interfacial contact between dye-adsorbed TiO_2 surface and the polymer gel electrolyte. Recently, researchers are trying to incorporate some micro- or nanofillers

A part of this chapter is published

S. Sharma, M. Khannam, M. Boruah, B.C. Nath, S.K. Dolui, *IEEE J. Photovolt.* 2015, 5(6), 1665-1673.

into the gel electrolyte that can reduce their drawbacks, thus enhancing the performance of the cell.[5-7] The use of nanostructures in solar cells facilitates the performance of the cell by offering large surface area and unique optical effects by the method of anti-reflection and reducing the charge recombination by improving the electron transport through the nanostructures.[8] In addition, various factors, such as size, shape, concentration, and crystallinity of the nanofiller and bonding between the polymeric gel and the nanofiller play an important role in enhancing the photovoltaic performance of the polymer.[9-11] Now-a-days, anisotropic nanocrystals have drawn growing attention because of their unique properties arising from various aspect ratios.[12-14] But still a few works are found that deal with the photovoltaic properties of a polymer gel electrolyte in a set of DSSCs, where the aspect ratios of the nanocrystals has a notable impact on device performance.

Natural or synthetic biopolymers are suitable as a gel electrolyte in DSSCs because of their biocompatibility, biodegradability, and environmental friendliness. Among other biopolymers, gelatin is the most suitable and efficient due to its excellent film-forming properties by easy and simple methods.[15, 16] Metal nanoparticles, such as gold (Au), are interesting in the sense that they have the fascinating plasmonic properties arising from the collective oscillation of the conduction electrons under electromagnetic radiation. This phenomenon is confined near the boundary between the metal nanoparticle and the surrounding polymer that causes enhancement in optical absorption.[17] Au nanoparticles are chemically highly stable, and at the same time, they are biocompatible, have low toxicity, and have easy-to-form homogeneous particles. With these advantages, Au nanoparticle is a promising candidate for solar cell applications. The addition of Au nanoparticles into a gel electrolyte facilitates the enhancement of ionic conductivity of the gel by providing a large active surface area. As a result, it provides outstanding electrocatalytic activity for the I_3^-/I^- reaction with enhanced device performance.[5, 10]

In the present chapter, an attempt has been made to synthesize a series of new composite electrolytes incorporating Au nanorods with various aspect ratios as the nanofiller into gelatin matrix for application into DSSCs. The DSSCs fabricated with highest aspect ratio Au nanorods at concentration of 0.04% show significantly

improved photo conversion efficiency (PCE) of 1.98%, in comparison with the DSSC fabricated with pristine gelatin.

4.2 Experimental

4.2.1 Reagents

The chemicals including gelatin (from porcin skin), chloroauric acid ($HAuCl_4$), glutaraldehyde, acetonitrile, tertiary butylpyridine (TBP), 1-methyl-3propyl imidazolium iodide (MPII), lithium iodide (LiI), cis-bis(isothiocyanato)bis(2,2-bipyridyl-4,4-dicarboxylato) ruthenium (II) bis-tetrabutylammonium (N-719) and fluorine-doped tin oxide (FTO)-coated glasses (Sheet resistance: 15 Ω/sq) were purchased from Sigma Aldrich India. N-methyl 2-pyrrolidone (NMP), ethanol, acetone, sodium borohydride ($NaBH_4$), cetyltrimethyl ammonium bromide (CTAB) and ascorbic acid were purchased from Merck India. Silver nitrate ($AgNO_3$) was purchased from Rankem.

4.2.2 Synthesis of Au nanorods

To study the effect of size and shape of Au nanorods on the device performance, a set of three samples with different anisotropic Au nanorods was prepared using a two-step procedure developed earlier.[18] Here, the concentrations of growth solution were varied to control the shape as well as aspect ratio. In the first step, the seed solution was prepared by adding 0.60 mL of freshly prepared and ice cold 0.01 M $NaBH_4$ solution to a mixture of CTAB (5 mL, 0.2 M) and $HAuCl_4$ solution (5 mL of 0.001292 M). The resulting brownish yellow solution indicated the successful formation of Au seeds. Next step is the formation of different aspect ratio Au nanorods using the pre-synthesized seed solution. First, CTAB (5 mL, 0.20 M) was added to 0.25, 0.15, 0.05 mL of 0.0040 M $AgNO_3$ solution at room temperature, followed by the addition of 5 mL of 0.0010 M $HAuCl_4$ under gentle mixing. The concentrations of Ag^+ ion in the growth solution were 9.8×10^{-5} M, 5.9×10^{-5} M, and 2.03×10^{-5} M for 0.25, 0.15, and 0.05 mL of 0.0040 M $AgNO_3$ solution, respectively. To the stirred solution, 70 μL of 0.0788 M ascorbic acid was added. Being a mild reducing agent, ascorbic acid slowly changes the colour of the growth solution from dark yellow to colourless. The final step was the addition of 12 μL of the seed solution to the growth solution at room

temperature. The colour of the solution gradually changed within 10-20 min and the colour change takes place more slowly for higher aspect ratio nanorods. The temperature of the growth medium was kept constant at room temperature in all the experiments. In addition, in all the nanoparticle dispersion, some spherical particles cannot grow during the reaction. Therefore, anisotropic nanocrystals were centrifuged for several times and then re-dispersed in water to remove spherical nanoparticles, the reactants, and the stabilizing agents. The whole mechanism is described in the chapter 2 [Scheme 2.1].

4.2.3 Synthesis of Au/gelatin gel electrolyte

Gelatin gels with or without Au nanorods were synthesized by a two-step procedure. At first, 10% solution of gelatin was prepared by dissolving 1 g of gelatin in10 mL water at 50°C and the solution was allowed to stir for 20 min so that gelatin can be dissolved properly. During stirring different concentration (viz., 0%, 0.01%, 0.04%, and 0.06%) of pre-synthesized Au nanorods dispersion were added to the solution under vigorous stirring for 15-20 min. Finally, 1.5 mL of crosslinker (glutaraldehyde) was added to the mixture. After curing at 60-70 °C, the mixture turned into the desired nanocomposite gel within a few minutes. The products were washed properly with water several times to remove the un-reacted crosslinker from the surface of the gel, dried, and collected for analysis and further applications. The process is summarized in Scheme 4.1.

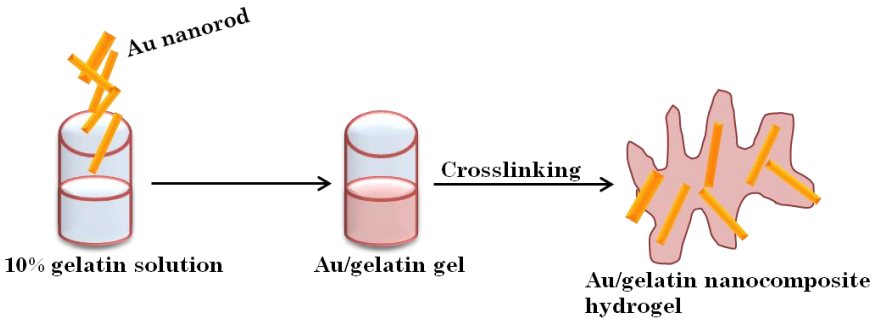

Scheme 4.1 Schematic representation of the formation of Au/gelatin nanocomposite hydrogel

A gel electrolyte was prepared by soaking 0.5 g of dried Au/gelatin gel in the liquid electrolyte for more than 96 h to reach absorption saturation. The liquid electrolyte comprises of a mixture of 0.1 M (LiI), 0.6 M I_2, 0.5 M TBP, 0.05 M MPII in a mixed solvent of NMP and acetonitrile with the 2:8 ratio.

4.2.4 Assembling of dye-sensitized solar cells

FTO-coated glass slides were first properly cleaned in a detergent solution using an ultrasonicator bath for 10 min, followed by rinsing with double distilled water, acetone, and ethanol and, finally, dried under N_2 atmosphere. A paste of nanocrystalline TiO_2 with ethanol was deposited onto FTO-coated glass by doctor blade technique, followed by sintering at 450 °C for 1 h. The sintered TiO_2 photoanodes were sensitized by immersing the films into a 0.3 mM N719 dye solution in a mixed solvent of acetonitrile and ethanol with a volume ratio of 1:1 for 24 h. Then, the electrodes were washed with ethanol and dried in air. The pre-synthesized Au/gelatin gel electrolyte was spread evenly on the dye adsorbed photoanode. Platinum (Pt) metal coated another FTO glass was taken as counter electrode, and this was placed over gel electrolyte. A device was fabricated using gel electrolytes incorporated with or without different aspect ratio Au nanorods. All the devices were kept at 70 °C for 10 min to allow the electrolyte to penetrate into the dye adsorbed TiO_2 layer prior to the photovoltaic measurements.

4.3 Instruments and methods

4.3.1 Transmission electron microscopy (TEM)

The morphological characteristic of the synthesized Au nanorods was investigated by transmission electron microscope (JEM 2100) with an acceleration voltage of 100-300 kV.

4.3.2 Scanning electron microscopy (SEM)

The surface morphology of the nanocomposite gel was revealed by JSM-6390LV scanning electron microscopy (SEM), JEOL, Japan.

4.3.3 Fourier transform infrared spectrometer (FT-IR)

Fourier transform infrared (FT-IR) spectra of the nanocomposite gel were recorded in FT-IR Nicolet, (Impact 410) spectrophotometer (USA). During analysis pellets were prepared by a compression moulding under vacuum, by using a required amount of

samples grounded and mixed properly with dried KBr. The spectra were recorded in transmission mode in the range of 4000-400 cm^{-1} with a nominal resolution of 4 cm^{-1}.

4.3.4 Ultraviolet-visible spectroscopy (UV-visible)

The solid state ultraviolet-visible (UV-visible) spectra of the nanocomposite gel were recorded in a UV-visible spectrophotometer (Model: Shimadzu UV-2550) in a wavelength ranges from 200 to 800 nm.

4.3.5 Electrochemical impedance spectroscopy (EIS)

Electrochemical impedance spectroscopy (EIS) is an experimental method of characterizing the electrochemical property of a gel electrolyte in quasi solid state DSSCs over a range of frequencies. Through EIS, we can analyze various electrocatalytic activities for the regeneration of a redox couple, such as electron transport in the TiO_2 electrode, electron transfer at the counter electrode, ion transport in the electrolyte, and the charge recombination at the TiO_2/dye/electrolyte interface.

The impedance analysis of fabricated DSSCs was performed on SP-150 Potentiostat Galvanostat electrochemical impedance workstation at a constant temperature of 25 °C with ac signal amplitude of 90-264 V in the frequency range from 4 Hz to 100 kHz.

4.3.6 Thermogravimetric analysis (TGA)

The thermal characteristic of the synthesized nanocomposite gel was revealed by Thermogravimetric analysis (TGA). Thermogravimetric data was taken in a Shimazdu TGA 50 thermal analyzer at a heating rate of 10 °C min^{-1} and a temperature ranges from 25 °C to 600 °C under nitrogen (flow rate: 30 mL min^{-1}).

4.3.7 Differential scanning calorimetry (DSC)

The glass-transition temperature of the synthesized nanocomposite gel was studied by differential scanning calorimetry (DSC) using a Shimadzu DSC-60 in nitrogen atmosphere. The analysis was run at a scanning speed of 10 °C min^{-1} from 25-250 °C.

4.3.8 Photovoltaic Test

The photovoltaic measurement of fabricated DSSCs was carried out under illumination

of a 100-mW/cm^2 solar simulator in ambient atmosphere and photovoltaic parameters were calculated using the following equations:

$$\text{Fill factor, FF} = \frac{J_{max}.V_{max}}{J_{sc}.V_{oc}} \qquad \text{Eqn. 4.1}$$

$$\text{Maximum power, } P_{max} = J_{max}.V_{max} = J_{sc}.V_{oc}.FF \qquad \text{Eqn. 4.2}$$

$$\eta = \frac{P_{max}}{P_{in}} = \frac{J_{sc}.V_{oc}.FF}{P_{in}} \qquad \text{Eqn. 4.3}$$

Where, J_{max} and V_{max} are the current density and voltage, respectively at the maximum power point of the photocurrent density versus voltage plot. J_{sc} and V_{oc} are the short-circuit current density and open-circuit voltage, respectively. FF is the fill factor. P_{in} is the intensity of the white light, and η is the PCE of the device.

4.4 Results and discussion

4.4.1 Morphology (TEM, SEM)

Fig. 4.1 represents the morphological image of synthesized Au nanorods from transmission electron microscopy (TEM). TEM image of Au nanorods prepared at a 2.03×10^{-5} M Ag^+ concentration shows an incomplete growth of nanocrystals

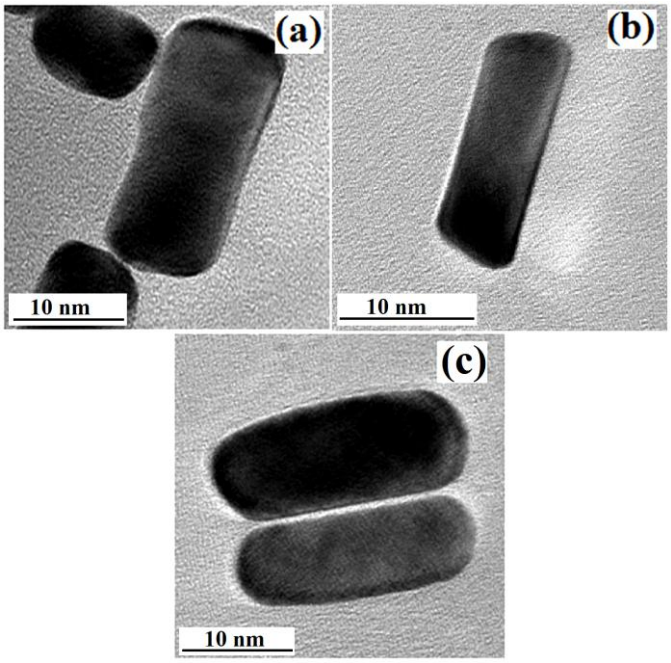

Fig. 4.1 TEM images of Au nanorods (a) AR-2, (b) AR-2.5 and (c) AR-3.5. *AR-aspect ratio

with an average aspect ratio of 2 [Fig. 4.1a]. With the increase in Ag^+ ion concentration, homogeneity in growth, as well as aspect ratio increases too. A homogeneous growth is observed for Au nanorods, prepared at 9.8×10^{-5} M Ag^+ concentration [Fig. 4.1c] with an average aspect ratio of 3.5. Addition of silver nitrate into the growth solution plays a major role in the growth of Au nanorods. During the reaction, $AgNO_3$ is added prior to addition of a mild reducing agent, like ascorbic acid due to which the acid reduces Ag^+ to Ag^0 in the solution. As the oxidation potential of Au^{3+} is lower than Ag^+, galvanic replacement occurs by forming Au^0 atoms and Ag^+ ions. Au^{3+} oxidizes three Ag^0 atoms and, therefore, with increase in Ag^+ ion concentration, more Au^0 atoms will form. After addition of the Au seed solution, a kinetically controlled reaction occurs where the seed particles act as the nucleation site for nanorod growth. The CTAB-capped seed behaves as a soft template and growth of nanorods starts by diffusing Au atoms into the template. As the Ag^+ ion concentration increases, more Au atoms will diffuse into the template, thus forming high aspect ratio nanorods.

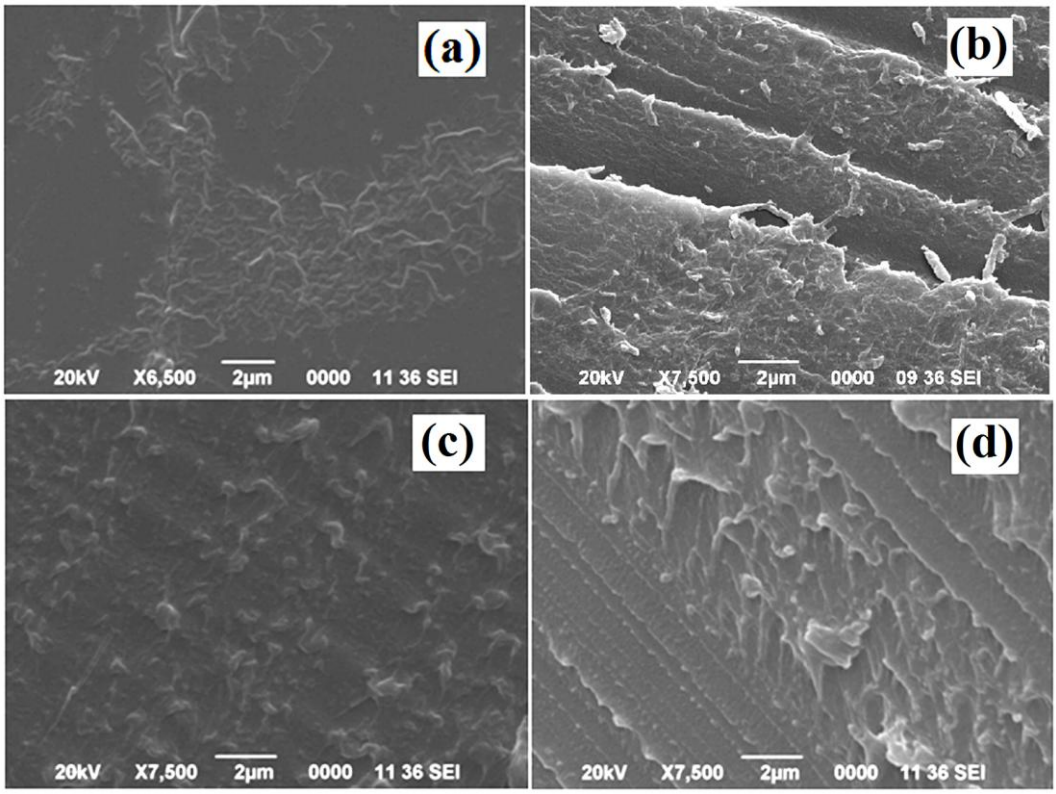

Fig. 4.2 Cross-sectional SEM images of (a) gelatin, (b) Au/gelatin (0.01%), (c) Au/gelatin (0.04%), and (d) Au/gelatin (0.06%). *number in the bracket is the concentration of nanorods

The cross-sectional scanning electron microscopy (SEM) images of bare gelatin and Au/gelatin gel electrolyte at three different concentrations of Au nanorods (AR-3.5) are shown in Fig. 4.2. The bare gelatin [Fig. 4.2a] shows the uniform surface with smooth morphology. However, the morphology dramatically changes with the addition of Au nanorods into the gelatin matrix [Fig. 4.2b-d]. More homogeneous and well-mixed morphology is observed for Au/gelatin gel electrolyte at Au concentration of 0.04%, in comparison with the gel at concentration 0.01% and 0.06%. The energy-dispersive X-ray spectrum (EDX) [Fig. 4.3] confirms the successful incorporation of Au nanorods into the gelatin network. The increase of Au content in the nanocomposites can be well understood by the EDX spectra [Fig. 4.3b-d].

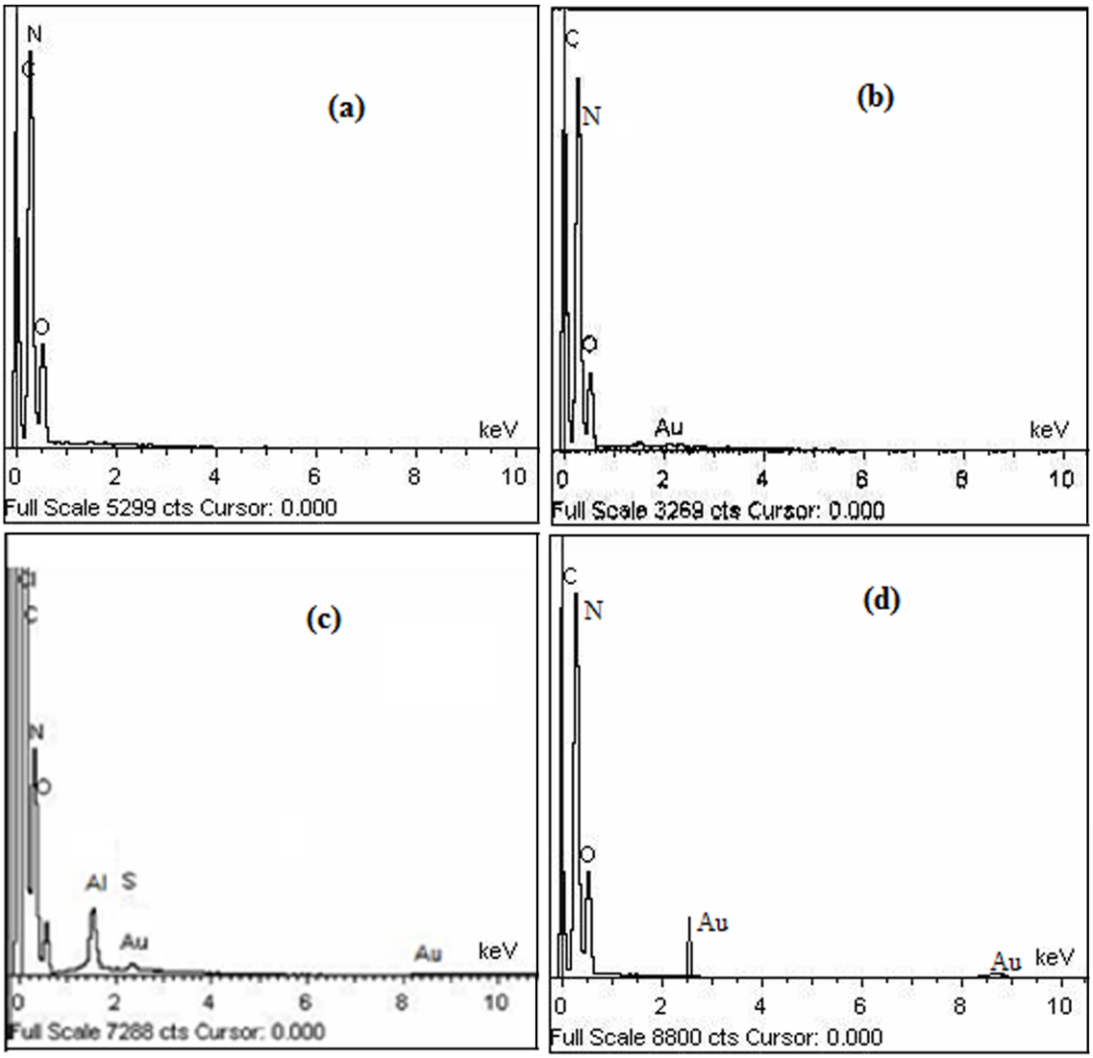

Fig. 4.3 EDX spectra of (a) gelatin, (b) Au/gelatin (0.01%), (c) Au/gelatin (0.04%), and (d) Au/gelatin (0.06%). *number in the bracket is the concentration of nanorods

4.4.2 Structural characteristics (FT-IR)

The formation of the nanocomposite gel is investigated by FT-IR [Fig. 4.4]. All the characteristic peaks reveal the formation of gelatin as well as Au/gelatin nanocomposite gel. Summary of the results is provided in Table 4.1. The characteristic peak at 1387 cm^{-1} arises from the aldimine absorption, which reveals proper crosslinking of gelatin.[19, 20] During crosslinking, the aldehyde group (–CHO) of glutaraldehyde reacts with the amino group ($–NH_2$) of the lysine residues of proteins, thus resulting in the formation of an aldimine linkage.[19] All the characteristic peaks shift towards higher wave number in the nanocomposites, which can be attributed to the presence of some degree of interaction of Au nanorods with gelatin due to which bonds become stronger in the nanocomposite compared to their pristine polymer gel. Moreover, in the finger print region, an absorption band is found at 418-422 cm^{-1} in all Au/gelatin nanocomposites [Fig. 4.4 inset], which is completely diminished in pristine gelatin. This band may be resulted from the presence of Au nanorods in close proximity of nitrogen atom in gelatin.

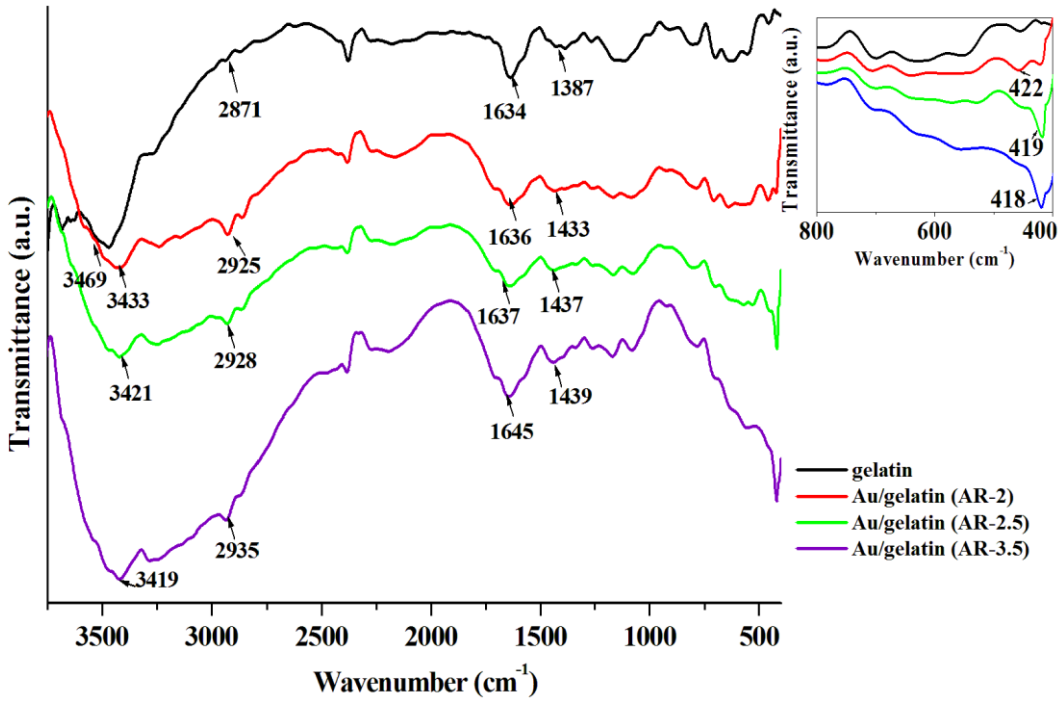

Fig. 4.4 FTIR spectra of gelatin and nanocomposite gel with different aspect ratio (AR) of Au nanorods. Inset shows the absorption peak of Au nanorods in the nanocomposites

Table 4.1 Characteristic vibrational modes for nanocomposite gel

Characteristic bond	Wavenumber (cm^{-1})			
	Gelatin	Au/gelatin (AR-2)	Au/gelatin (AR-2.5)	Au/gelatin (AR-3.5)
CH=N (aldimine) absorption	1387	1433	1437	1439
C=O stretching (amide)	1634	1636	1637	1645
C-H stretching (amide)	2871	2925	2928	2935
N-H stretching (amide)	3469	3433	3421	3419

*AR-aspect ratio of the nanorods

4.4.3 Optical characterization (UV-visible)

UV-visible spectra of neat gelatin and the Au/gelatin nanocomposites are depicted in Fig. 4.5. In the UV-visible spectrum of gelatin, a peak at around 287 nm is observed which is due to the $\pi \rightarrow \pi^*$ transition of aldimine linkage.[19, 21] This peak is also observed in the Au/gelatin nanocomposites with a slight shift in the absorption maxima. It implies that in the presence of Au nanorods, some sort of chemical modification

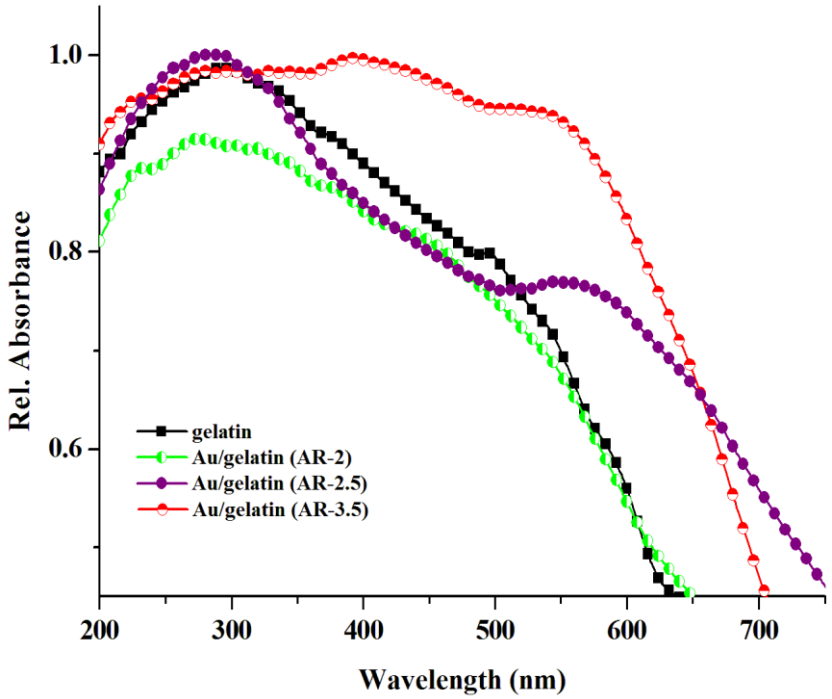

Fig. 4.5 UV-visible spectra of gelatin and nanocomposite gel with different aspect ratio (AR) of Au nanorods

around the aldimine linkage has taken place. This result is supported by FT-IR analysis [Fig. 4.4]. Another peak is observed in all the spectra of nanocomposites at around 531-540 nm, which arises from the surface plasmon resonance of Au nanorods.[22] It confirms the successful incorporation of Au nanorods into the gelatin network.

4.4.4 Evaluation of Electrochemical properties (EIS)

Electrochemical impedance spectroscopy (EIS) is proven to be the most efficient tool for investigating the interfacial charge transfer resistance of gel electrolytes in DSSCs. Through EIS, we can analyze various electrocatalytic activities for the regeneration of a redox couple, such as electron transport in the TiO_2 electrode, electron transfer at the counter electrode, ion transport in the electrolyte, and the charge recombination at the TiO_2/dye/electrolyte interface[23, 24] We carried out the EIS analysis of the fabricated devices by exposing them to the constant AM 1.5 G 100 mW/cm^2 illumination. Fig. 4.6 shows the Nyquist plot of fabricated gelatin gel-based devices. Under illumination and biased condition, in the high-frequency range, a small semicircle occurs, which corresponds to the charge transfer resistance at the counter electrode/electrolyte interface (R_{ct1}). Another larger semicircle occurs at low-frequency range, which is governed by the charge transfer resistance (R_{ct2}) at the electrolyte/TiO_2 electrode interface.[5] We have also measured the series resistance (R_s), associated with the electrolyte and electric contacts in the fabricated devices. All the measured parameters are summarized in Table 4.2.

It is observed that the R_{ct2} for Au/gelatin gel electrolyte is smaller than their pristine counterpart, which is due to the decrease in resistance in the migration of ions in the electrolyte and electrode in presence of Au nanorods that provide remarkable electrocatalytic activity for the I_3^-/I^- reaction.[5] The charge transfer process and also the migration of ions (I^-/I_3^-) in the electrolyte increases, which arises from the increased interfacial contact between electrolyte and TiO_2 layer provided by the large active surface area of Au nanorods in the nanocomposites. With the increase in aspect ratio of Au nanorods, both the active surface area and electrocatalytic activity have a pronounced effect that promotes more reduction of R_{ct1} and R_{ct2}, thus improving the migration of ions and charge transfer process to a large extent. The large interfacial contact between the electrolyte and TiO_2 layer promotes the migration of ions and

transport of electrons through different channel, thus facilitating the enhancement of J_{sc} in the devices as shown in Fig. 4.8, and consequently, the fill factor increases for the high aspect ratio nanorods.[25, 26] These results are supported by the previous literature.[27, 28]

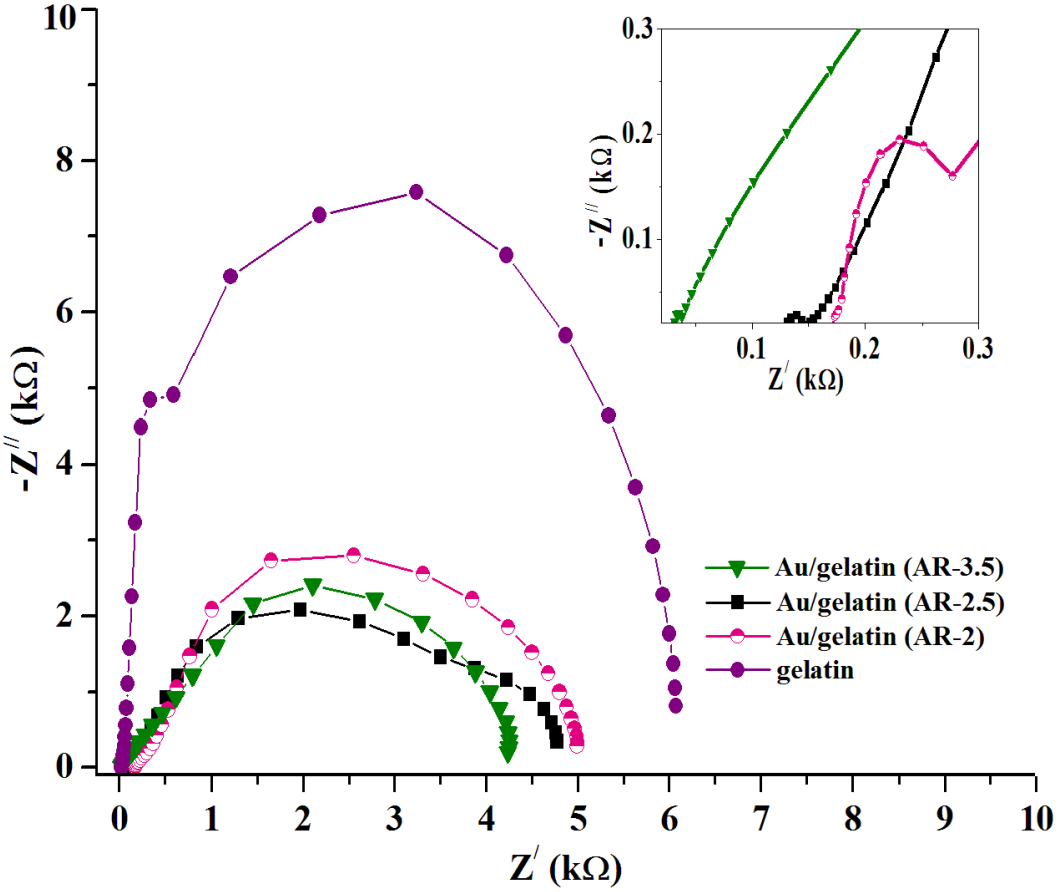

Fig. 4.6 EIS analysis spectra under illumination of gel electrolyte with different aspect ratio (AR) of Au nanorods. Inset shows the expansion of the area indicated by the circle

Table 4.2 Various parameters determined by EIS measurements of the original gel electrolyte and au/gelatin nanocomposite gel electrolytes

Device	R_s (kΩ)	R_{ct1} (kΩ)	R_{ct2} (kΩ)	δ (Scm^{-1})
Gelatin	0.19	0.57	6.04	$3.29x10^{-3}$
Au/gelatin (AR-2)	0.17	0.08	4.74	$3.67x10^{-3}$
Au/gelatin (AR-2.5)	0.13	0.02	4.63	$4.91x10^{-3}$
Au/gelatin (AR-3.5)	0.03	0.01	4.21	$2.24x10^{-2}$

*AR-aspect ratio of the nanorods

4.4.5 Study of thermal properties (TGA, DSC)

One of the most important properties in nanocomposite-based gel electrolytes is their thermal property. The thermal stability of the Au/gelatin gel electrolytes is investigated by using TGA and the weight loss traces recorded in the temperature range 25-600 °C as shown in Fig. 4.7(a). In addition, the TGA values of the nanocomposite and pristine gelatin are summarized in Table 4.3.

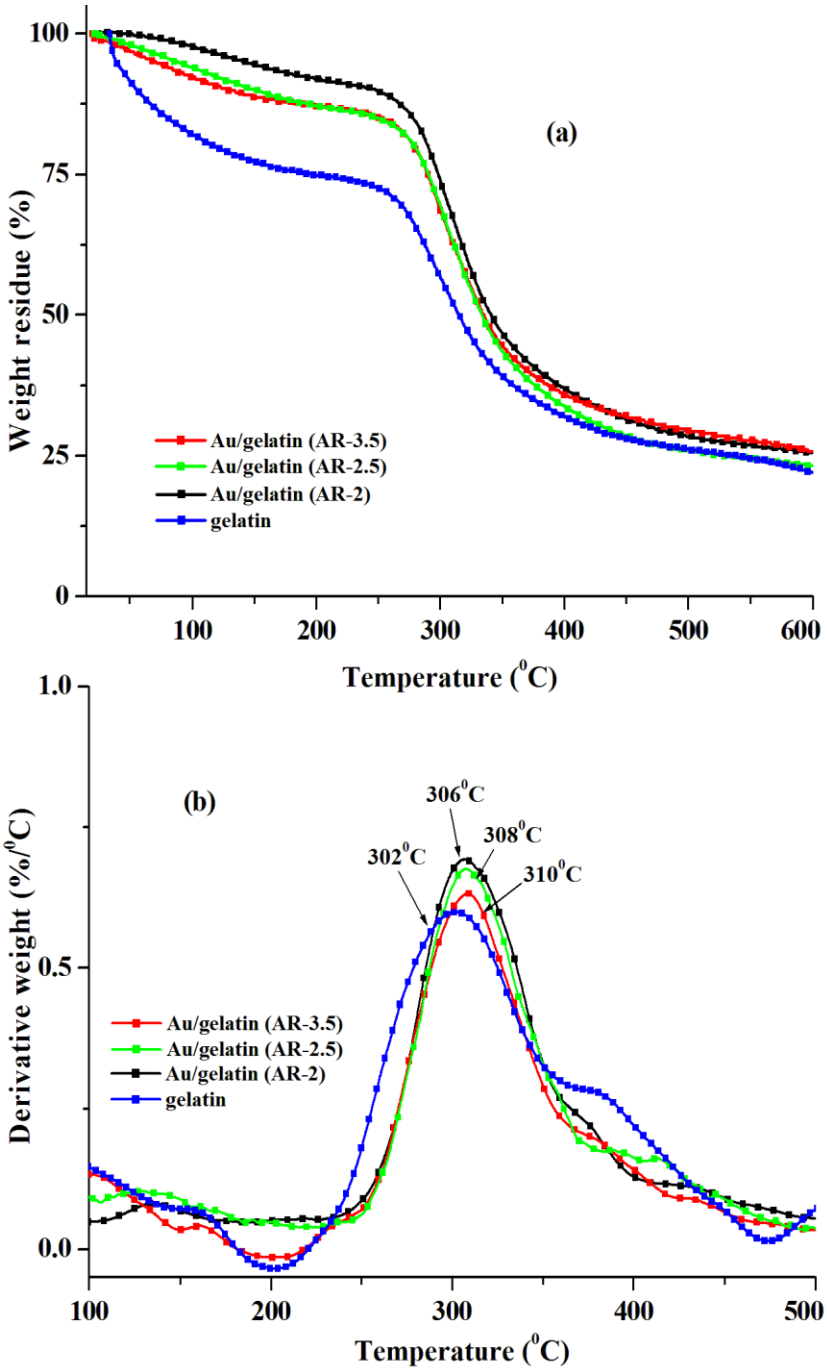

Fig. 4.7 (a) TGA and DTG curves of gelatin and nanocomposite gel with different aspect ratio (AR) of Au nanorods

An improvement in the thermal stability of the nanocomposite can be observed for all Au/gelatin nanocomposite gel. Major degradation starts in the range 193-357 °C for the gelatin and the major degradation temperature (T_d) is 302 °C. On the other hand, major degradation starts at remarkably higher temperature, in the range 226-420 °C for all the nanocomposite gels. Thermal degradation of polymers, in general, is initiated with the formation of free radical at the weak bonds or chains ends, followed by radical transfer to adjacent chains via inter chain reactions. The improved thermal stability in the nanocomposite can be attributed to the reduced mobility of the polymer chains, which suppressed the chain transfer reaction. Consequently, the degradation process is delayed and decomposition takes place at higher temperature.[29] The observed behaviour is most likely the consequence of the strong interaction between Au nanorods and gelatin matrix. Moreover, the incorporation of Au within the gelatin gel acts as a mass transport barrier to the volatile products generated during degradation process and increases the overall thermal stability of the nanocomposite gel.[29-31]

The aspect ratio of nanorods has a significant impact on thermal stability of gelatin.

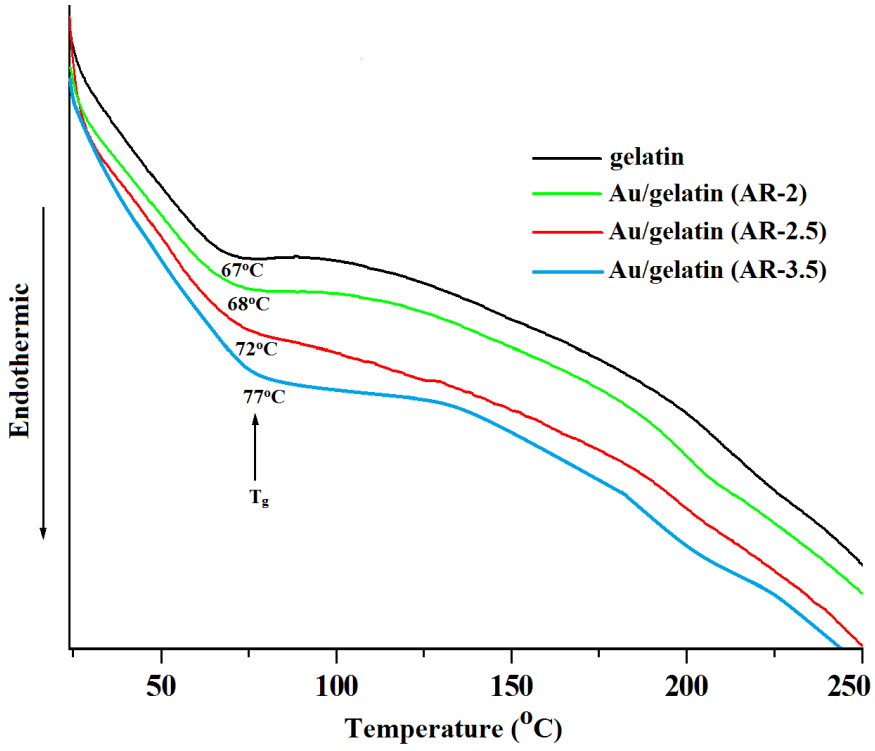

Fig. 4.8 DSC traces of polymer and nanocomposite gel with different aspect ratio (AR) of Au nanorods

From differential thermograms (DTG) [Fig. 4.7b], it is observed that the position of T_d shifts toward higher temperature with increasing the aspect ratio of nanorods. This observation is qualitatively consistent with the increase in glass transition temperature (T_g) with increasing the aspect ratio [Fig. 4.8]. Nanofiller present in the gelatin gel may limit the motion of polymer segments. With increasing the aspect ratio, this effect is more prominent. Thus, the interaction of polymer end groups with the produced free radicals is inhibited too some extent more effectively, which causes suppression of chain transfer reactions.[31] Again, the high aspect ratio Au create more effective mass transport barrier to the volatile products, thereby increasing the overall thermal stability of the nanocomposite gel.[29, 31]

Table 4.3 Thermal data from TGA and DSC

Sample particulate	Major degradation range (°C)	T_d (°C)	T_g (°C)
Gelatin	193-357	302	67
Au/gelatin (AR-2)	226-359	306	68
Au/gelatin (AR-2.5)	238-378	308	72
Au/gelatin (AR-3.5)	244-420	310	77

*AR-aspect ratio of nanorods

4.4.6 Photovoltaic performance evaluation

Photovoltaic characteristics of the fabricated DSSCs using Au/gelatin gel electrolytes, having different aspect ratio Au nanorods, are measured under 100 mW/cm^2 illumination. The parameters are summarized in Table 4.4 and also compared with that of the pristine gelatin. From Fig. 4.9(a), it is observed that photocurrent densities (J_{sc}), as well as PCE of the devices, are larger than their pristine counterpart, which can be attributed to the higher electrocatalytic activity of these gel electrolytes. These results can be correlated with the ionic conductivity data [Table 4.2]. The addition of Au nanorods into the gelatin network facilitates the enhancement of ionic conductivity by providing a large active surface area and outstanding electrocatalytic activity for the I_3^-/I^- reaction, thus resulting in the enhancement of J_{sc} and PCE.[5, 10] The incorporation of Au nanorods into gelatin network provides a bridge for the transport of charge species. In a gel electrolyte-based DSSC, it is in general expected that under the

influence of the electric field, the I^-/I_3^- redox couple accomplishes a series of oxidation and reduction reactions. The electron generated in the redox reaction is

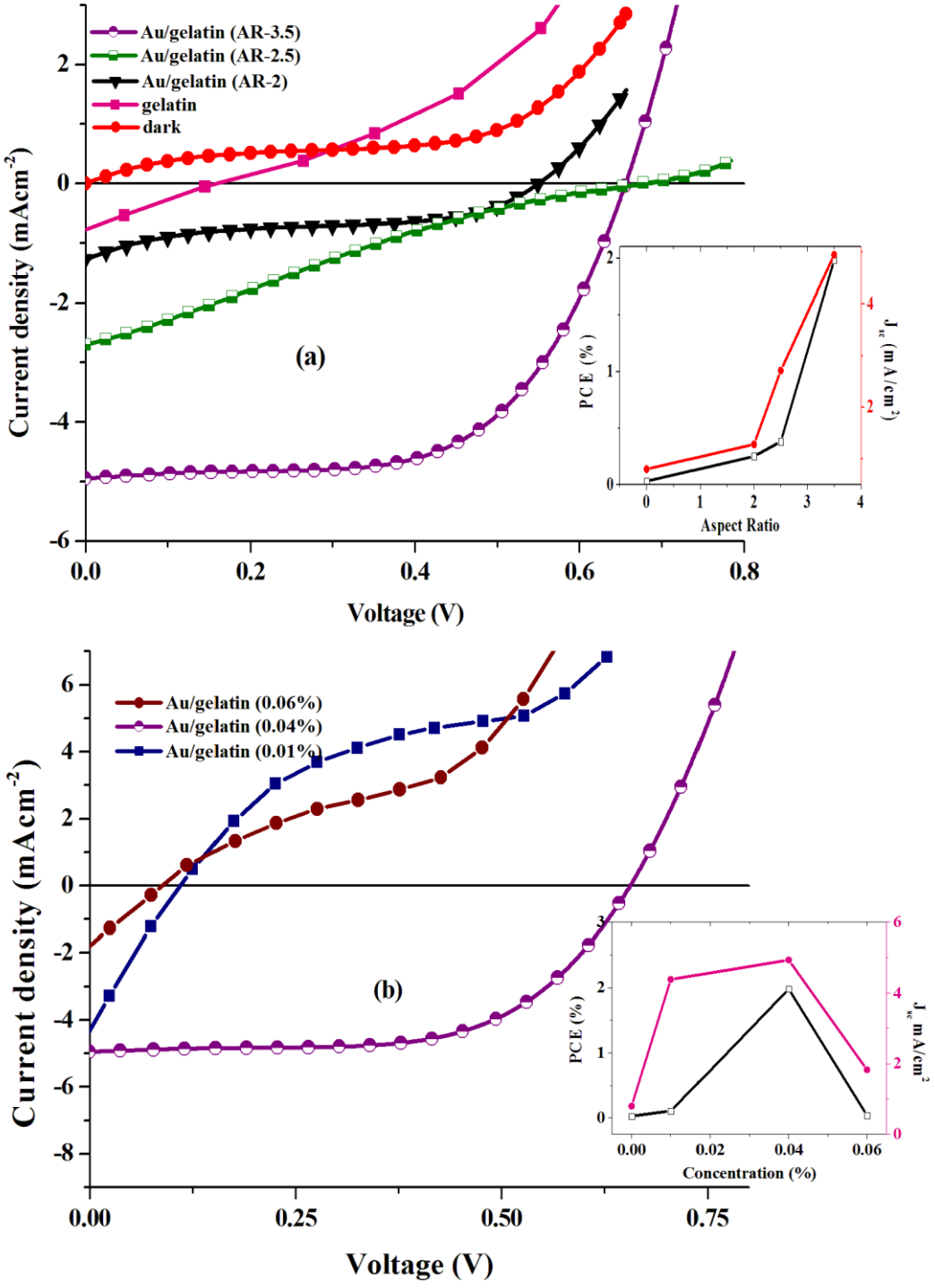

Fig. 4.9 J-V curves of gelatin and nanocomposite gel under illumination (a) with different aspect ratio (AR) of Au nanorods, inset shows effect of AR on PCE and J_{sc}; (b) at different concentration of Au nanorods of AR-3.5, inset shows effect of concentration on PCE and J_{sc}

transported through the Au nanorods. In other words, it can be said that Au nanorods can reduce the charge recombination rate and results increased in V_{oc} and J_{sc} of the nanocomposite devices. The transport mechanism of the fabricated device is shown schematically in Fig. 4.10a. The enhanced rate of collection and transport of electrons through different channel facilitates the enhancement of J_{sc} in the devices.[5, 25, 26] The dependence of PCE, as well as J_{sc} on the aspect ratio of Au nanorod is shown in Fig. 4.9a inset. From the figure, it is confirmed that the higher Au nanorods show increased value of photocurrent and PCE. Due to the significantly large active surface area and excellent electrocatalytic activity of high aspect ratio nanorods, the possibility of electron collection and transport through a different channel is enhanced, which may increase J_{sc} and PCE as well. For instance, when the aspect ratio is increased from 2.5 to 3.5, J_{sc} shows an increased value from 2.708 to 4.94 $mAcm^{-2}$.[32, 33] In all the nanocomposite devices, the V_{oc} and fill factor have almost similar values. Therefore, it can be inferred that the increased value of J_{sc} significantly improves the PCE of the devices. These results are supported by the previous studies.[27, 28]

We also studied the effect of concentration of nanofiller on the device performance, and results were summarized in Table 4.5. From the results, it is observed that PCE, V_{oc}, and J_{sc} increase up to an optimum nanorods concentration of 0.04% [Fig. 4.9b]. A further increase in concentration to 0.06% causes a steep decrease in device parameters, which may be due to the formation of solid networks in gel electrolyte with the excess nanorods. The effective surface area for the electron transfer from the counter electrode to the electrolyte is hindered due to formation of this solid network, as this network is in contact with the counter electrode. This renders the decrease of interfacial charge transfer value of the DSSCs.[5]

Table 4.4 Photovoltaic characteristics of DSSCs with different aspect ratio (AR) of nanorods

Device	V_{oc} (V)	J_{sc} (mA/cm^2)	FF	PCE, η (%)
Gelatin	0.16	0.8	0.23	0.03
Au/gelatin (AR-2)	0.55	1.28	0.36	0.25
Au/gelatin (AR-2.5)	0.62	2.71	0.23	0.38
Au/gelatin (AR-3.5)	0.66	4.94	0.61	1.98

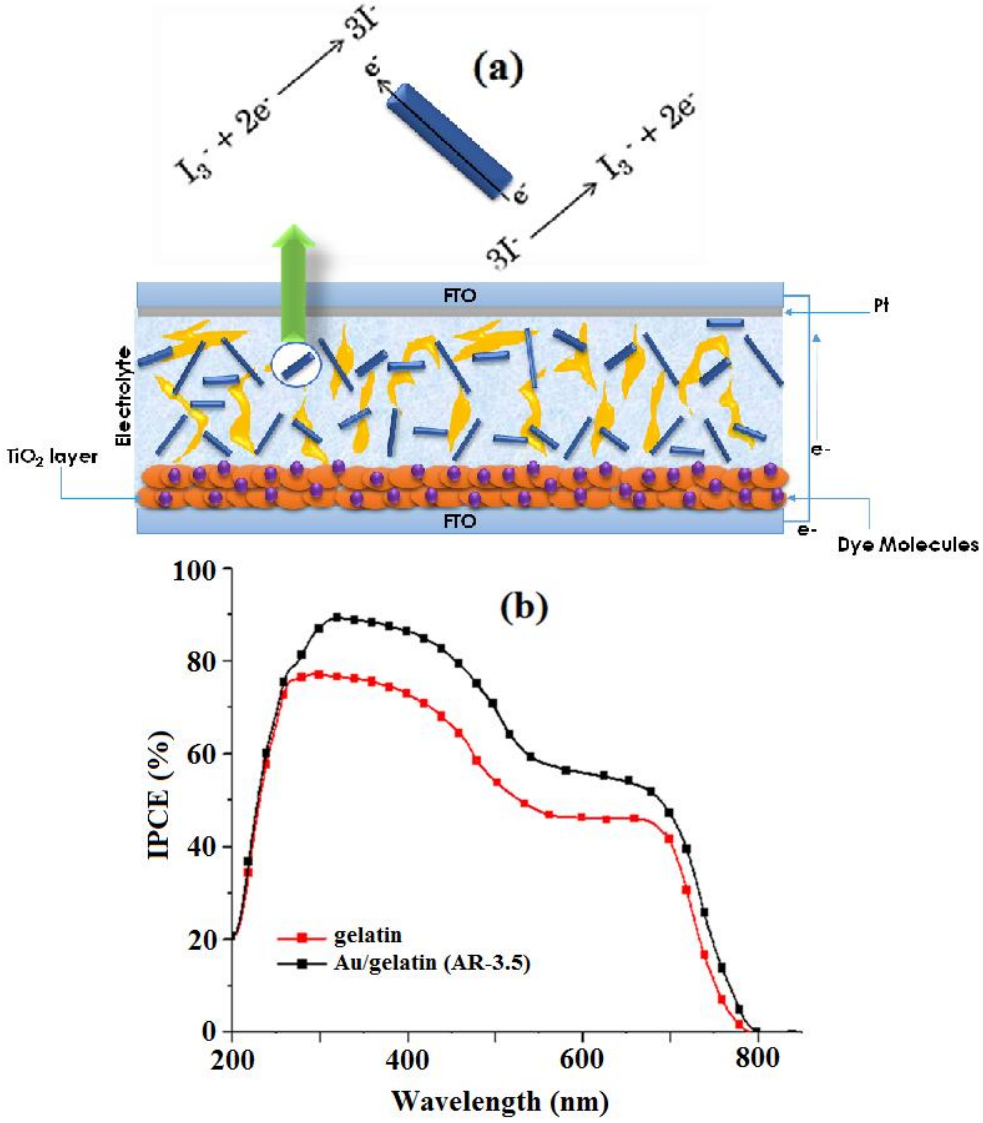

Fig. 4.10 (a) Electron transport mechanism in the fabricated device, (b) IPCE spectra of gelatin and nanocomposite gel with Au nanorod of aspect ratio (AR) 3.5

Table 4.5 Photovoltaic characteristics of DSSCs with different concentration of Au nanorods

Device	V_{oc} (V)	J_{sc} (mA/cm^2)	FF	PCE, η (%)
Au/gelatin (AR-3.5)-0.01%	0.11	4.39	0.22	0.11
Au/gelatin (AR-3.5)-0.04%	0.66	4.94	0.61	1.98
Au/gelatin (AR-3.5)-0.06%	0.09	1.83	0.24	0.04

*AR-aspect ratio of nanorods

The incident photon conversion efficiency (IPCE) spectrum of the photovoltaic device using Au/gelatin gel electrolyte (aspect ratio 3.5) is shown in Fig. 4.10b, and it is

compared with their pristine polymer gel. Spectrum shows a broad spectral response of the gel electrolyte in the range 200-800 nm with a maximum of IPCE value of 89%, which is quite larger than their pristine polymer (77%). This broader response implies a better light harvesting ability of the nanocomposite gel.[24]In order to study the stability of the fabricated DSSCs, we have performed a stability test for the cell, and results were compared with that for a liquid electrolyte-based cell reported in earlier studies.[34] and the results are summarized in Fig. 4.11. It is observed that the PCE of the gel electrolyte-based devices is decreased by only about 3.2% (from 1.98% to 1.91%) after 720 h [Fig. 4.11], whereas for liquid electrolyte-based devices, PCE is decreased by about 13% [Fig. 4.11] after the same period of time. During the study, the devices were stored under dark at 65 °C and 85% relative humidity. Under such a condition, dye molecules start desorbing from the TiO_2 photoanode under the effect of the solvent. Moreover, solvent in the electrolyte starts evaporating. In case of the gel electrolyte, evaporation is somewhat reduced because the electrolyte is entrapped into the gel network that prevents solvent leakage and evaporation. Moreover, the gel nanocomposite prevents desorption of dye molecules from the TiO_2 photoanode, thus providing better stability of the devices.

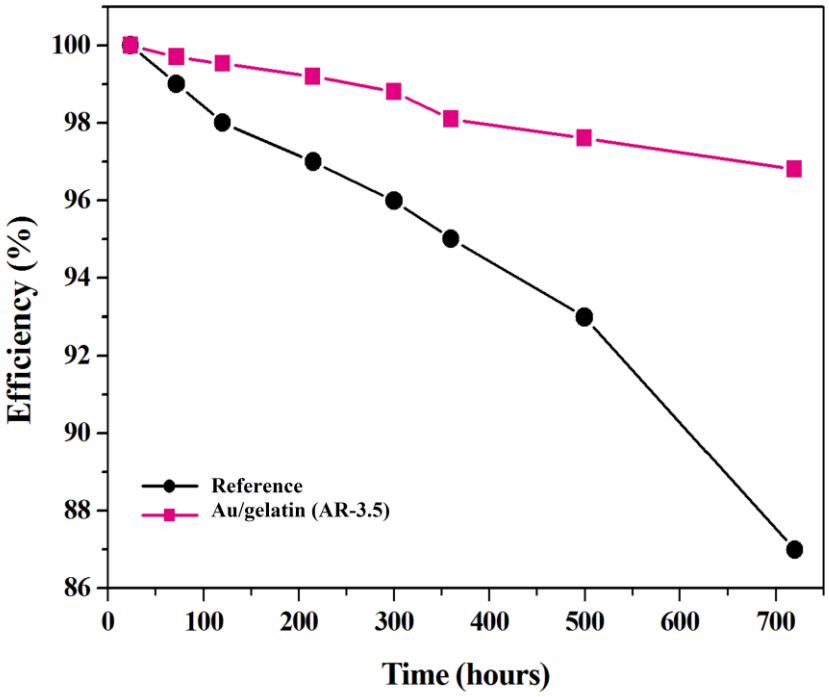

Fig. 4.11 Stability graph of the fabricated device

4.5 Conclusion

- We have demonstrated the seeded growth method of synthesis of various aspect ratio Au nanorods and immobilized in gelatin gel electrolyte.
- A set of DSSC based on Au/gelatin gel electrolyte was developed.
- The incorporation of high aspect ratio Au nanorods into gelatin results in the enhancement of device parameters, mainly in V_{oc}, J_{sc} and PCE due to the reduction of charge recombination and resistance in the electrolytes.
- The enhanced rate of collection and transport of electrons through different channel facilitates the enhancement of J_{sc} in the devices.
- At an optimum concentration of 0.04%, maximum PCE is obtained. Further increase in concentration causes a steep decrease in device parameters. This can be attributed to the formation of solid networks with the excess nanofiller that hinders the effective surface area for the electron transfer from the counter electrode to the electrolyte. This renders decrease in interfacial charge transfer value of the DSSCs.
- Overall, the result of this study suggests that Au nanorod of aspect ratio 3.5 is the best candidate for obtaining a PCE of 1.975% in a quasi-solid-state DSSC at 0.04% Au content.

References

1. Benedetti, J.E., et al. *J. Power Sources* **195**, 1246-1255, 2010.
2. Bandara, T.M.W.J., et al. *Electrochim. Acta* **55**, 2044-2047, 2010.
3. Kuang, D., et al. *J. Am. Chem. Soc.* **128**, 7732-7733, 2006.
4. Akhtar, M.S., et al. *Electrochim. Acta* **55**, 2418-2423, 2010.
5. Nath, B.C., et al. *Electrochim. Acta* **146**, 106-111, 2014.
6. Wei, D., et al. *Nanotechnology* **19**, 424006(1-5), 2008.
7. Xiong, H., et al. *Electrochim. Acta* **88**, 100-106, 2013.
8. Zhang, Q., et al. *Chem. Soc. Rev.* **42**, 3127-3171, 2013.
9. Usui, H., et al. *J. Photochem Photobiol A: Chem.* **164**, 97-101, 2004.
10. Akhtar, M.S., et al. *Electrochem. Commun.* **9**, 2833-2837, 2007.
11. Lai, Y.H., et al. *Sol. Energy Mater. Sol. Cells* **94**, 668-674, 2010.
12. Kwon, T., et al. *ACS Macro Lett.* **3**, 398-404, 2014.
13. Qian, X., et al. *Nanoscale Res. Lett.* **3**, 303-307, 2008.
14. Zhang, X., et al. *Sci. Rep.* **4**, 4596(1-8), 2014.
15. Arvanitoyannis, I.S. *Formation and properties of collagen and gelatin films and coatings* in *Protein-Based Films and Coatings*, A. Gennadios, eds., CRC Press, Boca Raton, 2002, 275-304.
16. Gennadios, A., McHugh, T.H., Weller, C.L., & Krochta, J.M. *Edible coating and films based on proteins* in *Edible Coatings and to Improve Food Quality*, J.M. Krochta, E.A. Baldwin, and M.O. Nisperos-Carriedo, eds. Technomic, Chicago, 1994, 201-277.
17. Harun, N.A., et al. *Nanoscale* **5**, 3817-3827, 2013.
18. Nikoobakht, B., & El-Sayed, M.A. *Method Chem. Mater.* **15**, 1957-1962, 2003.
19. Nguyen, T.H., & Lee, B.T. *J. Biomed. Sci. Eng.* **3**, 1117-1124, 2010.
20. Narbat, M.K., et al. *Iran. Biomed. J.* **10**, 215-223, 2006.
21. Pavia, D.L., Lampman, G.M., & Kriz, G.S. *Introduction to Spectroscopy*, 3rd ed. New York, 2001.
22. Sharma, S., et al. *Adv. Mater. Lett.* **6**, 235-241, 2015.
23. Miyashita, M., et al. *J. Am. Chem. Soc.* **130**, 17874-17881, 2008.
24. Chen, J.H., et al. *J. Org. Chem.* **76**, 8977-8985, 2011.
25. Chang, Y.H., et al. *J. Mater. Chem.* **22**, 15592-15598, 2012.

26. Wang, Y.C., et al. *J. Mater. Chem.* **22**, 6982-6989, 2012.

27. Cheema, H., et al. *Phys. Chem. Chem. Phys.* **17**, 2750-2756, 2015.

28. Wang, H., et al. *Beilstein J. Nanotechnol.* **3**, 378-387, 2012.

29. Gogoi, P., et al. *J. Appl. Polym. Sci.* **132**, 41490(1-9), 2015.

30. Apostolov, A.A., et al. *J. Appl. Polym. Sci.* **71**, 465-470, 1999.

31. Patra, N., et al. *Composites: Part B, Eng*. **43**, 3114-3119, 2012.

32. Lee, K.M., et al. *Sol. Energy Mater. Sol. Cells* **92**, 1628-1633, 2008.

33. Li, Q., et al. *Electrochem. Commun.* **10**, 1299-1302, 2008.

34. Yoon, J., et al. *J. Power Sources* **201**, 395-401, 2012.